# Inverse Method 3-D Reconstruction of Localized *in vivo* Fluorescence—Application to Sjøgren Syndrome

Victor Chernomordik, David Hattery, *Student Member, IEEE,* Israel Gannot, and Amir H. Gandjbakhche

***Abstract*— The development of specific fluorescently labeled cell surface markers have opened the possibility of specific and quantitative noninvasive diagnosis of tissue changes. We are developing a fluorescence scanning imaging system that can perform a "noninvasive optical biopsy" of the Sjøgren syndrome (SS) which may replace the currently used histological biopsy. The diagnosis of SS is based on the quantification of the number of topical preadministered fluorescent antibodies which specifically bind to the lymphocytes infiltrating the minor salivary glands. We intend to scan the lower lip, and for each position of the scan, generate a two-dimensional (2-D) image of fluorescence using a charge-coupled device (CCD) camera. We have shown previously that our diffuse fluorescent photon migration theory predicts adequately the positions and strengths of one and two fluorescent targets embedded at different depths in tissue-like phantoms. An inverse reconstruction algorithm based on our theoretical findings has been written in C$^{++}$ and uses 2-D images to predict the strength and location of embedded fluorophores. However, due to large numbers of variables, which include the optical properties of the tissue at the excitation and emission wavelengths, and the positions and strengths of an unknown number of fluorophore targets, the validity of the final result depends on assumptions (such as the number of targets) and the input values for the optical parameters. Our results show that the number of fluorophore targets reconstructed for each scan is limited to two, and at least the scattering coefficient at the excitation wavelength is needed *a priori* to obtain good results. The latter can be obtained by measurements of spatially resolved diffuse reflectance at the excitation wavelength that provides the product of the absorption and scattering coefficients.**

***Index Terms*—Diffusion processes, fluorescence, image reconstruction, inverse problems, molecular tagging, random media, tissue optics.**

## I. Introduction

THE SPECIFIC fluorescently labeled cell surface markers used in confocal or near field microscopy have proven successful at imaging internal cell activity and imaging near tissue surfaces [1]. However, because of the highly scattering property of almost all tissue-types, when fluorescent targets lie deeper than 1 mm within the tissue, quantification of fluorophore concentration cannot be obtained simply from surface images of intensity [2], [3]. Thus, one has to devise image reconstruction techniques that are based on a theoretical framework which describes photon path dispersion within tissue [4]–[9].

We have chosen a salivary gland disease, Sjøgren syndrome (SS), as a test case to study the feasibility of noninvasive quantitative fluorescent imaging for the diagnosis and monitoring of this pathology. SS [10] meets the following minimum requirements for a clinically practical imaging study: 1) the pathology under investigation must not lie at a depth where the attenuation of the signal gives poor signal-to-noise ratio (SNR) and resolvability: for SS the minor salivary glands are located at a depth between 1–3 mm; 2) the specificity of the marker must be such that one can clearly distinguish between normal and abnormal lesions: for SS, fluorescent IL2 antibodies will bind to the activated lymphocytes and the degree of their infiltration into the salivary glands is a sole criterion of definitive diagnosis; and 3) the site of the optical biopsy, here the lower lip, is easily accessible for imaging. Our concept is to excite the fluorescent molecules by a scanning laser beam and to collect a series of fluorescent images with a cooled charge-coupled device (CCD) camera via a fiber bundle. From the two-dimensional (2-D) images, we will use our inverse algorithms to map the three-dimensional (3-D) distribution of the fluorescent IL2 antibodies in the lip, quantify their concentration, and relate the latter to the diagnosis of SS.

In a set of experimental and theoretical studies, we have shown that results based on our diffuse fluorescent photon migration theory are in very good agreement with the intensity profiles obtained experimentally for one and two fluorophores embedded at differing depths and different distances between the laser source and the fluorophore(s) location [11]. Although the agreement between the theoretical findings and experimental results (i.e., forward problem) is the prerequisite for devising a reconstruction algorithm, mapping of the 3-D location of unknown numbers of fluorophores (i.e., the inverse problem) needs its special assumptions and strategy. This is due essentially to the large number of parameters involved in the reconstruction scheme. In the next section, we present the characteristics of the algorithm written in C$^{++}$ followed

Manuscript received July 13, 1999; revised July 23, 1999.

V. Chernomordik, and A. H. Gandjbakhche are with the Laboratory of Integrative and Medical Biophysics, National Institute of Child Health and Human Development, National Institutes of Health, Bethesda, MD 20892 USA.

D. Hattery is with the Laboratory of Integrative and Medical Biophysics, National Institute of Child Health and Human Development, National Institutes of Health, Bethesda, MD 20892 USA. He is also with the Department of Electrical and Computer Engineering, George Washington University, Washington, DC 20052 USA.

I. Gannot is with the Biomedical Engineering Department, Faculty of Engineering, Tel-Aviv University, Tel-Aviv 69978, Israel.

Publisher Item Identifier S 1077-260X(99)07536-X.

by actual data obtained using this algorithm. Based on these findings, the last section is dedicated to the refinement of the algorithm and the scheme chosen for our analysis.

## II. Forward Problem

We have shown previously that when laser light impinges tissue at a point, (0, 0, 0), the fluorescent signal emitted from a fluorescent site at $\mathbf{s} = (\overline{x}_f, \overline{y}_f, \overline{z}_f)$, and detected at the tissue surface at $\mathbf{r} = (\overline{x}, \overline{y}, 0)$ can be written as shown in (1) (found at the bottom of the page) [3], [12]. In this equation, $\mu_a$ and $\mu'_s$ are the absorption and effective scattering coefficients. The subscripts $i$ and $e$ stand for incident and emitted light, and $\mu_{af}$ and $\mu'_{sf}$ are the optical coefficients of the fluorescent site. The parameter $\Phi$ is the probability that an excited fluorophore will in fact emit a fluorescent photon, i.e., it is the quantum efficiency (note that for biological media fluorescence $\Phi$ is much less than one). $c$ is the speed of light. $H(\alpha, \beta)$ is the function

$$H(\alpha, \beta) = \frac{1}{\sqrt{\alpha\beta}} \exp\left\{-2\left[\sqrt{\alpha\left(\frac{\mu_{ai}}{\mu'_{si}}\right)} + \sqrt{\beta\left(\frac{\mu_{ae}}{\mu'_{se}}\right)}\right]\right\} \tag{2}$$

where

$$\alpha_{\pm} = \frac{3}{4}\left[\overline{x}_f^2 + \overline{y}_f^2 + \left(\overline{z}_f \pm \overline{z}_0\right)^2\right]\left(\mu'_{si}\right)^2 \tag{3}$$

$$\beta_{\pm} = \frac{3}{4}\left[\left(\overline{x}_f - \overline{x}\right)^2 + \left(\overline{y}_f - \overline{y}\right)^2 + \left(\overline{z}_f + \overline{z}_0 \pm \overline{z}_0\right)^2\right]\left(\mu'_{se}\right)^2 \tag{4}$$

where $\overline{z}_0 = \sqrt{2}\,\mu_s^{-1}$.

In the case where several fluorescent sites are embedded in tissue, the simplest analysis assumes that the detected signal is merely the sum of signals emitted from each site.

Experiments have been performed on phantoms made of Delrin in which ground rhodamine fluorescent targets mixed with Delrin powder was poured into predrilled holes. The size of each target was 1 mm$^3$. In order to create different depths for the fluorescent targets, the Delrin block was covered with Delrin slabs of 1–6 mm thickness in 1-mm steps. A schematic of the experimental setup is shown in Fig. 1. An Argon laser (488 nm) excited the rhodamine target(s) (1 mm$^3$). The fluorescent light was then collected by a CCD camera after filtering and sent to a computer for image processing (e.g., correction for the nonlinearity of the CCD). Details of the image processing are presented elsewhere [11].

In experiments with a single fluorophore site, 66 images corresponding to 11 source-target separations (from 0 to 10 mm, 1-mm steps) for 6 different depths (1–6 mm, 1-mm steps) of the site were acquired [11]. Experiments with two fluorophore sites were performed in the same way. Three

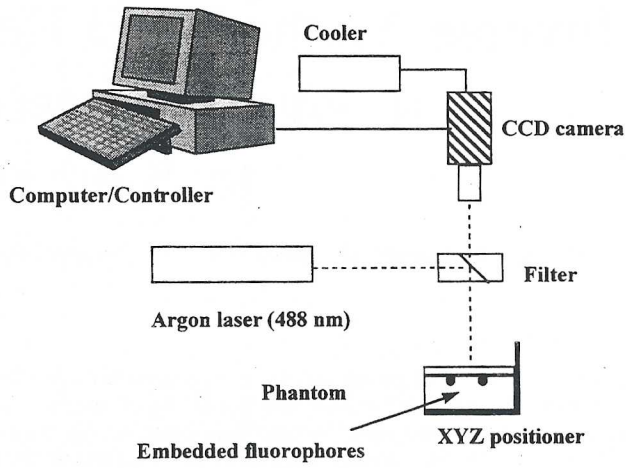


Fig. 1. Schematic drawing of the image acquisition system.

sets of phantoms were made in which the distance between the centers of the fluorophores were 1.5, 2.5, and 3.5 mm, respectively.

The optical properties of the Delrin slabs at the incident and emitted wavelengths were deduced using measurements of total reflectance and transmittance using the method of integrating spheres. In this method the total reflectance and total transmittance of the slabs with known thickness are measured, and the optical properties $\mu_a$ and $\mu'_s$ are derived using an inverse algorithm based on random walk theory [11]. For Delrin, the method yielded: $\mu_{ai} = 0.008$ mm$^{-1}$, $\mu_{ae} = 0.004$ mm$^{-1}$, $\mu'_{si} = 2.7$ mm$^{-1}$, and $\mu'_{se} = 1.6$ mm$^{-1}$.

We have tested the forward problem by inserting the known parameters of the experimental phantoms into the theoretical expression given in (1) for each of the configurations [e.g., different target depths and distances between the laser source and the target(s)]. Very good agreements between the experimental results and the theoretical expression were found [3], [11]. In Fig. 2(a) and (b), examples of this agreement are shown. In Fig. 2(a), line scan data retrieved from 2-D images, corresponding to fluorophores at 1 mm depth with differing distances between the laser source and the fluorophores are shown. Clearly when the lateral distance between the laser source and the fluorophore(s) increases, the maximum signal is attenuated. However, because the fluorophores are at the same depth, the normalized intensities should have the same shape. This feature is illustrated in Fig. 2(b) in which the theoretical fit to the data is also shown. We have investigated features of the theory, such as the ratio of the intensities obtained for two fluorophores at two different depths, and the falloff of intensity as a function of source-fluorophore lateral separation. Moreover, we have shown that in the case of two fluorophores, the theory gives similarly good agreement [3], [11].

$$\Gamma(\mathbf{r}, \mathbf{s}) = \frac{\Phi\frac{\mu_{af}}{\mu'_{sf}}\left[H(\alpha_-, \beta_-) - H(\alpha_-, \beta_+) - H(\alpha_+, \beta_-) + H(\alpha_+, \beta_+)\right]\exp\left[-(\mu_{ae}/\mu'_s)\right]}{\left[1 - \frac{\mu_{af}}{\mu'_{sf}} + \frac{\mu_{af}}{\mu'_{sf}}\left[1 + \frac{1}{8}\left(\frac{3}{\pi}\right)^{3/2}\sum_{m=1}^{\infty}\frac{1}{m^{3/2}}\exp\left[-2m\left(\frac{\mu_{ai}}{\mu'_{si}}\right)\right]\right]\right]} \tag{1}$$

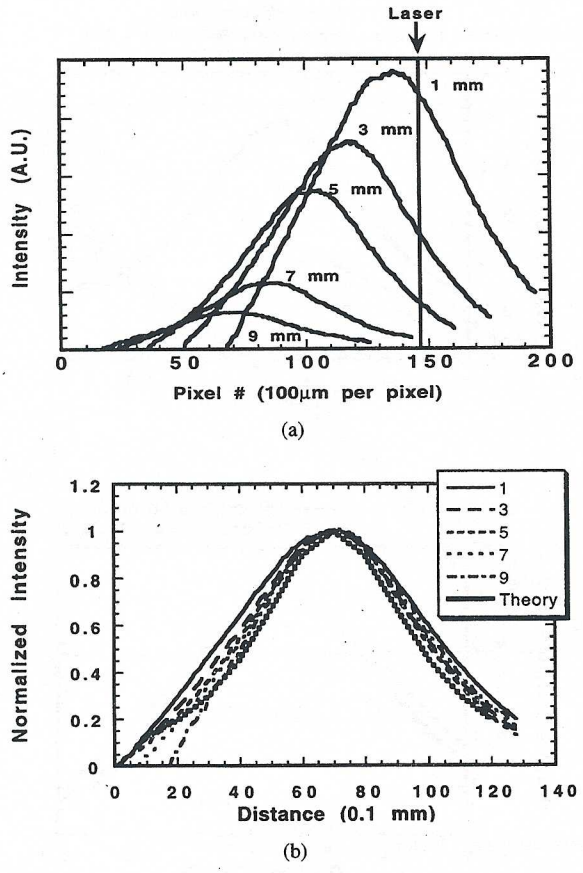


Fig. 2. (a) Fluorescent emission intensity profiles detected at the surface directly above a single, 1-mm$^3$ fluorescent mass at 3-mm depth in a Delrin slab. The radial distance between the laser spot and the fluorophore is indicated for each curve. (b) Normalized and translated curves of the emission profiles in Fig. 2(a) and the LRW model to show profile similarity.

However, as we will see below, the large number of parameters involved requires some assumptions and knowledge of specific parameters for a successful 3-D mapping of fluorescent sites.

## III. Inverse Problem

An inverse algorithm, based on our theoretical expressions, has been written in C$^{++}$ to determine positions of fluorescent inclusions and their relative strengths (in the case of several fluorophore sites) from measured 2-D intensity distributions, $I(x, y)$, recorded by a CCD camera. The known parameters of the inverse algorithm are the location of the laser source, dimensions of the detection field (in our case: $12.8 \times 12.8$ mm$^2$), and step interval of the scanning, $\Delta s = 0.1$ mm (after reduction of acquired raw image of $512 \times 512$ pixels to $128 \times 128$ pixels). Equations (1)–(3) presented above depend on the four optical parameters of the medium (scattering and absorption at the excitation and emission wavelengths), and three coordinates with an amplitude (product of the quantum efficiency, fluorophore absorption, and its concentration) for each fluorophore site. Assuming constant fluorescent absorption and quantum efficiency, the amplitude(s) can be assumed to be directly proportional to the concentration of fluorophore at a particular site.

Our inverse algorithm is based on a multiparameter curve fitting procedure that compares the theoretical expressions with experimental data. To facilitate this, we first reduce our problem from 2-D to 1-D by introducing an auxiliary variable, $U = (x/\Delta s)n_{sc} + y/\Delta s$, that replaces the $x$ and $y$ coordinates of an image pixel ($n_{sc}$ being the number of pixels in each scan). The resulting function with one variable is curve fit using the standard Levenberg–Marquardt method.

Testing the robustness of the reconstruction procedure requires two critical elements. First, the number of optical parameters needed to estimate the depth and the concentration of the fluorophores. Second, an estimate of the number of embedded fluorophores. The fitting parameters are coordinates of fluorescent inclusions ($x_i$, $y_i$, $z_i$, $i \leq 3$), their strengths $A_i$, background intensity $I_0$, and the optical characteristics of the medium: $\mu_{ai}$, $\mu_{ae}$, $\mu'_{se}$, and $\mu'_{si}$. We have used images obtained for cases of one fluorophore target and attempted to reconstruct the location of that fluorophore by letting the algorithm vary all of the parameters. As expected, no good agreement was found between the nominal value of the target's depth and that of reconstructed value. Note that in the case of one fluorophore, the $\{x, y\}$ position is the same as the location of maximum intensity in the 2-D image. In the next step, we used just the scattering coefficient at the incident wavelength, $\mu'_{si}$, as an input parameter (i.e., determined in advance) and let the algorithm vary all the remaining variables. The reconstructed depths for these cases were in very good agreement with the nominal values (data not shown). Finally, we have checked our algorithm for the simpler case in which all optical parameters are known and we have found that characteristics of fluorophores are practically the same as for the case in which only one optical parameter, namely $\mu'_{si}$, is known. This result shows that the scattering coefficient determines the scaling of all geometrical characteristics of inclusions. However, when just $\mu'_{si}$ is known, estimated values of the three unknown optical parameters, as determined by the curve fitting algorithm, differ from actual values.

The second critical element in the reconstruction is the number of fluorophore sites, $N_f$, inside the phantom which is an input parameter for our data processing. We can determine it directly only if all inclusions are far enough from each other to provide distinct peaks in the observed intensity distribution. However, for cases in which the distance between two fluorophores is less than, or on the order of, the actual depths, the image provided by two sites exhibits only one intensity peak. This case requires special analysis to distinguish between the presence of one or two fluorophore sites as presented below.

An experimental intensity scan in the $x$-direction for a single fluorophore at 2.5 mm depth is presented in Fig. 3 along with two reconstructed intensity profiles from this image using curve fitting assumptions $N_f = 1$ and $N_f = 2$, respectively. Reconstruction under assumption $N_f = 1$ (short dashed line) yields the correct values for the inclusion's lateral coordinates $x$ and $y$, as well as depth, $z = 2.46$ mm. If we add the second fluorophore to the fitting model, it somewhat improves the result using the $\chi^2$ metric ($(\Delta\chi^2/\chi^2) \lessapprox 75\%$), with the depth, $z = 2.51$ mm of the first fluorophore close to the actual depth of the fluorophore. However, a second fluorophore is

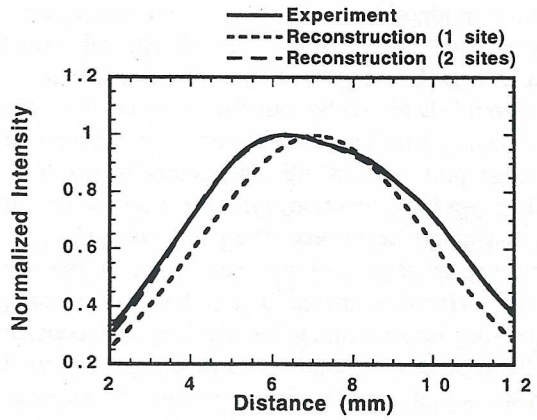


Fig. 3. Intensity scan for one fluorophore at depth 2.5 mm shown with reconstructed curves using assumptions of one and two fluorophore sites.

"reconstructed" at depth $z = 3.55$ mm, and lateral location $x > 10.5$ mm which is clearly wrong. The concentration ratio of the two reconstructed fluorophores is 0.34. Though from experimental data alone we cannot exclude the presence of the second fluorophore, by looking at the concentration ratio and the location of the second fluorophore in the image field, we can ascertain that there is only one fluorophore.

To the contrary, for the phantom containing two fluorophores much better agreement between experimental data and fitted intensity distribution is evident for assumed $N_f = 2$ than $N_f = 1$ even if both fluorophores in the phantom are close enough to each other in the $\{x, y\}$ plane, so as to produce only one peak in the measured intensity distribution. In Fig. 4(a) and (b), for example, experimental intensity scans in both $x$- and $y$-directions for two fluorophores at depth $z = 3.5$ mm and with 3.5 mm lateral separation are presented, along with two reconstructed intensity profiles obtained from curve fitting under assumptions $N_f = 1$ (short dashed line) and $N_f = 2$ (long dashed line). As seen in Fig. 4(a), fitting with $N_f = 2$ gives better agreement with the data than when one fits with $N_f = 1$, as expected. However, one cannot make a definitive suggestion about the number of fluorophore(s). On the other hand, the $y$-scan data [Fig. 4(b)] shows that the asymmetry involved in the case of two embedded fluorophores manifests clearly in the reconstruction procedure. Reconstruction under assumption $N_f = 2$ gives the right values for lateral coordinates $x$ and $y$, as well as depth $z$ of both inclusions and their relative strength (with error $\lessapprox 10\%$). The position of the single fluorophore found under the flawed $N_f = 1$ assumption is close to averaged positions of two real inclusions.

Overall performance of our inverse algorithm is given in Tables I and II. These results are the worst case in more than 20 reconstructions performed on our experimental data. In these tables, we compare some results of the inverse problem solution with experimental characteristics of the phantom containing two fluorophores (depths of inclusions and ratio of concentrations, corresponding to the ratio of observed relative intensity). Reconstructed parameters are presented for two versions of curve fitting: one optical parameter of the medium ($\mu'_{si}$) is known and all four parameters ($\mu_{ai}$, $\mu_{ae}$, $\mu'_{si}$, and $\mu'_{se}$) are known. It can be seen from these tables that our data

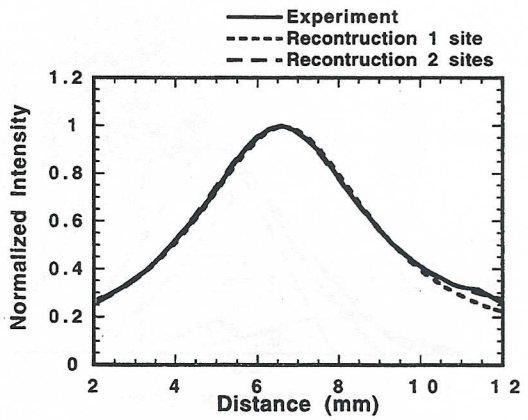


(a)

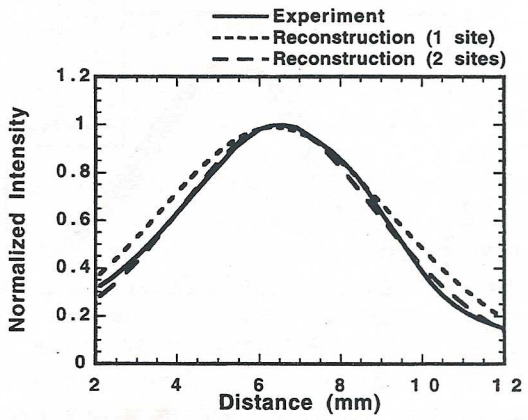


(b)

Fig. 4. (a) Intensity scan in $x$-direction of two fluorophores at depth 3.5 mm and separation 3.5 mm in $y$-direction shown with reconstructed curves using assumptions of one and two fluorophore sites. (b) Intensity scan in $y$-direction of two fluorophores at depth 3.5 mm and separation 3.5 mm in $y$-direction shown with reconstructed curves using assumptions of one and two fluorophore sites.

TABLE I
RECONSTRUCTED FLUOROPHORE DEPTHS USING A SINGLE KNOWN OPTICAL PARAMETER, AND USING FOUR KNOWN OPTICAL PARAMETERS

| Depth (mm) | Depth (mm) (1 parameter) | | Depth (mm) (4 parameters) | |
|---|---|---|---|---|
| 1.5 | 1.8 | 2.0 | 1.7 | 1.9 |
| 2.5 | 2.6 | 3.0 | 2.5 | 2.7 |
| 3.5 | 4.1 | 4.5 | 3.5 | 3.9 |

TABLE II
RECONSTRUCTED FLUOROPHORE INTENSITY RATIOS USING A SINGLE KNOWN OPTICAL PARAMETER AND USING FOUR KNOWN OPTICAL PARAMETERS

| Depth (mm) | Ratio Forward | Ratio 1 Parameter | Ratio 4 parameters |
|---|---|---|---|
| 1.5 | 1.33 | 1.41 | 1.45 |
| 2.5 | 1.51 | 1.61 | 1.6 |
| 3.5 | 1.47 | 1.54 | 1.6 |

processing algorithm provides good estimates (with error $\lessapprox$ 20%) for all characteristics in question for these phantoms with either one or two fluorophores.

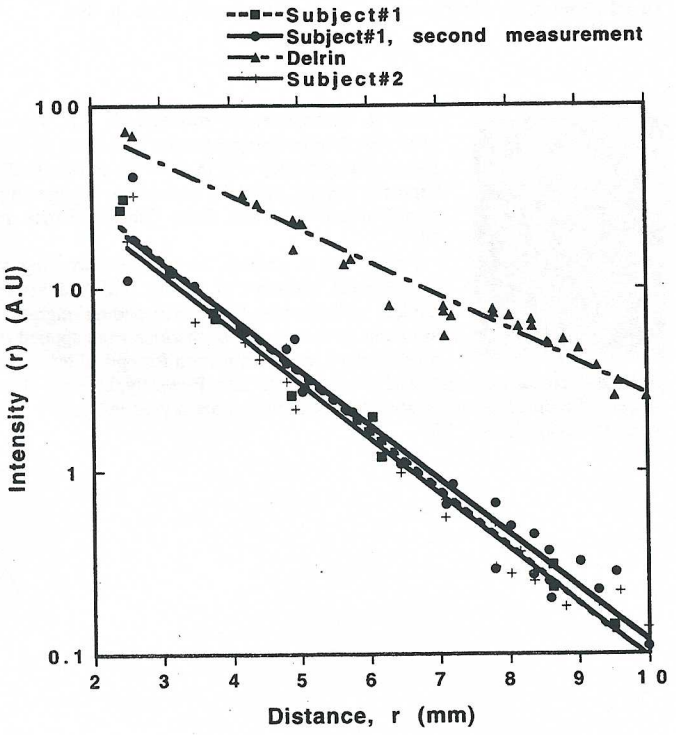


(a)

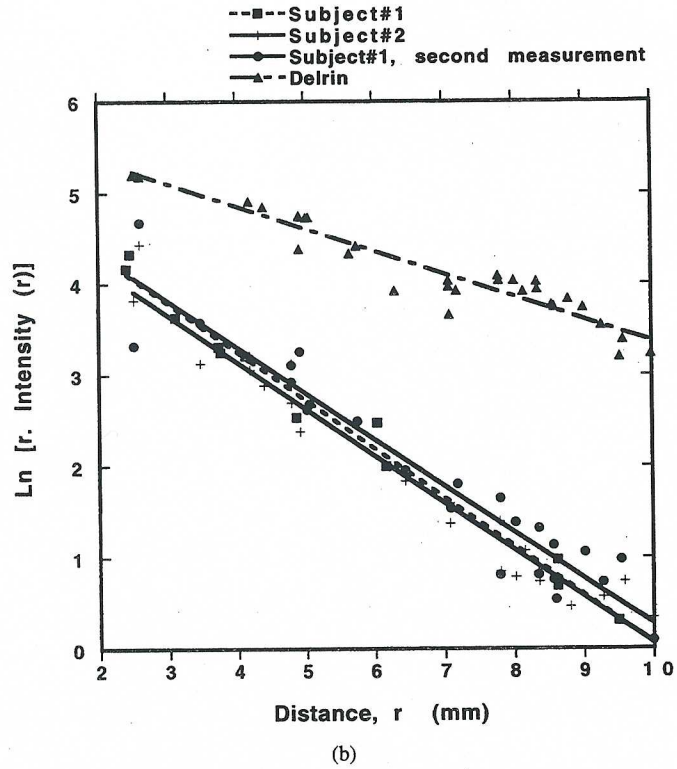


(b)

Fig. 5. (a) Measurements of 633 nm intensity for source-detector separations, $r$, of the lips of two subjects. (b) Log plot of $r$ times intensity of values in Fig. 5(a).

## IV. Summary and Discussion

Our ultimate goal is to reconstruct fluorophore locations and concentrations from intensity scans of a tissue surface. Our method requires multiple images which must be chosen in a way to include no more than two fluorophore sites. Our inverse algorithm can then reconstruct the depth and the concentration of one or two fluorophores. Moreover, using a symmetry in orthogonal line scans, the algorithm is able to distinguish whether one or two fluorophores are included in an intensity peak in the image. There are degenerate cases for which the algorithm cannot distinguish between one and two fluorophores. Two important examples are when the two fluorophores are in the same lateral position and differ only in depth, and when they are laterally very close to each other. In both of these cases, no asymmetry will manifest in the image.

We have shown that reasonable reconstruction of the concentration and depth of fluorophores requires the knowledge of at least one of the scattering coefficients and that this coefficient determines the scaling of the background. To obtain one of these coefficients, one can use the imaging system to acquire spatially resolved reflectance at the excitation and/or the emission wavelengths from which the product of $\mu_a\ \mu_s'$ can be deduced using the exponential fall-off of the reflectance [9]. To demonstrate this ability, we have measured the spatially resolved diffuse reflectance, $I(r)$, of the lower lip of two subjects with a He–Ne laser (633 nm), where $r$ is the distance between the laser source and the detector as seen in Fig. 5(a). In Fig. 5(b), $Ln(rI(r))$ is shown as a function of $r$. The slope of this quantity is equal to $\sqrt{3\mu_a\mu_s'}$ from which the product of $\mu_a\ \mu_s'$ can be obtained. One can calibrate the reflectance measuring device using a Delrin slab, and then calculate the total reflectance from the lip and deduce $\mu_a$ and $\mu_s'$. The knowledge of the latter value is sufficient for accurate reconstruction.

Finally, the inverse algorithm presented in this paper can be applied to many diseases for which specific *in situ* fluorescent molecular markers are being developed.

## References

[1] J. M. Schmitt, A. Knüttel, and M. Yadlowsky, "Confocal microscopy in turbid media," *J. Opt. Soc. Amer.*, vol. 11, pp. 2226–2235, 1995.

[2] A. H. Gandjbakhche, R. Nossal, and R. F. Bonner, "Resolution limits for optical transillumination of abnormalities embedded in tissues," *Med. Phys.*, vol. 22, pp. 185–191, 1994.

[3] A. H. Gandjbakhche and I. Gannot, "Quantitative fluorescent imaging of specific markers of diseased tissue," *IEEE J. Select. Topics Quantum Electron.*, vol. 2, pp. 914–921, Dec. 1996.

[4] J. A. Moon and J. Reintjes, "Image resolution by use of multiply scattered light," *Opt. Lett.*, vol. 19, pp. 521–523, 1994.

[5] J. Wu, M. S. Feld, and R. P. Rava, "Analytical model for extracting intrinsic fluorescence in turbid media," *Appl. Opt.*, vol. 32, pp. 3585–3595, 1993.

[6] E. M. Sevick-Muraca and C. Hutchinson, "Probability description of fluorescent and phosphorescent signal generation in tissues and other random media," in *Proc. Advances in Laser and Light Spectroscopy to Diagnose Cancer and Other Diseases*, R. R. Alfano, Ed. San Jose, CA,: SPIE, 1995, vol. 2387.

[7] M. S. Patterson and B. Pogue, "A mathematical model for time-resolved and frequency-domain fluorescence spectroscopy in biological tissue," *Appl. Opt.*, vol. 33, p. 1963, 1994.

[8] R. F. Bonner, R. Nossal, S. Havlin, and G. H. Weiss, "Model for photon migration in turbid biological media," *J. Opt. Soc. Amer. A*, vol. 4, pp. 423–432, 1987.

[9] A. H. Gandjbakhche and G. H. Weiss, "Random walk and diffusion-like model of photon migration in turbid media," in *Progress in Optics*, E. Wolf, Ed., 1995, vol. 34, pp. 333–402.

[10] R. I. Fox, Ed., "Sjøgren syndrome," *Rheumatic Disease Clinic of North America*, 1992.

[11] I. Gannot, R. F. Bonner, G. Gannot, P. C. Fox, P. D. Smith, and A. H. Gandjbakhche, "Optical simulations of a noninvasive technique for the

diagnosis of diseased salivary glands *in situ*," *Med. Phys.*, vol. 25, pp. 1139–1144, 1998.

[12] A. H. Gandjbakhche, R. F. Bonner, R. Nossal, and G. H. Weiss, "Effects of multiple passage probability on fluorescent signals from biological media," *Appl. Opt.*, vol. 36, pp. 4613–4619, 1997.

**Victor Chernomordik** received the M.S. and Ph.D. degrees, both in theoretical physics, from Moscow Institute of Physics and Technology, Moscow, Russia. His Ph.D. work concerned physical processes in the intergalactic medium.

Currently he is working at the Laboratory of Integrative and Medical Biophysics, NICHD, National Institutes of Health, Bethesda, MD. His present research interests are: tissue optics; development of algorithms to solve inverse problems and determine parameters of abnormal inclusions in highly scattering media; and application of neutron and X-ray scattering to analyze macromolecular scattering assemblies.

**David Hattery** (S'94) received the M.S.E.E. degreee from Texas A&M University, College Station, TX, in 1991, and the B.A. degree in physics from Indiana University, Bloomington, IN, in 1982. He is working toward the D.Sc. degree in biomedical engineering at George Washington University, Washington, DC.

He is an ARCS Fellow and is currently researching tissue optics for his dissertation at the National Institutes of Health (NIH). Before switching his focus to medical imaging, he was a Navy reconnaissance and fighter pilot who flew F-14 Tomcats.

**Israel Gannot**, for photograph and biography, see this issue, p. 894.

**Amir H. Gandjbakhche** received his B.S. degree in electrical engineering from the University of Science and Technology of Iran, in 1977, and the Ph.D. degree in physics, specialty biomedical engineering, from University of Paris, Denis Diderot, France, in 1989.

From 1990 to present, he has been working at the National Institutes of Health (NIH), devising random walk theories to describe photon migration in biological tissues. These theories were applied to time-resolved transillumination for optical tomography and fluorescence imaging of biological activities. Presently, he is the chief of unit of biomedical stochastic physics in the laboratory of integrative and medical biophysics at NIH.